Kirigami and the Caspar-Klug construction for viral shells with negative Gauss curvature

Luigi E. Perotti, Kevin Zhang, Joseph Rudnick, and Robijn F. Bruinsma

Kirigami and the Caspar-Klug Construction for Viral Shells with Negative Gauss Curvature

Luigi E. Perotti[*]

Department of Radiological Sciences, University of California, Los Angeles, CA 90095, USA and
Department of Bioengineering, University of California, Los Angeles, CA 90095, USA

Kevin Zhang[†]

Department of Mechanical and Aerospace Engineering,
University of California, Los Angeles, CA 90095, USA[‡]

Joseph Rudnick[§]

Department of Physics and Astronomy, University of California, Los Angeles, CA 90095, USA

Robijn F. Bruinsma[¶]

Department of Physics and Astronomy, University of California, Los Angeles, CA 90095, USA and
Department of Chemistry and Biochemistry,
University of California, Los Angeles, CA 90095, USA
(Dated: November 18, 2018)

In this work we extend the Caspar-Klug construction to the archaeal viruses, which in recent years have captured the attention of many researchers for their ability to thrive in extreme environments. We assume that the shells of archaeal viruses are composed of hexamers and pentamers — as it is true for icosahedral viruses — together with heptamers, necessary to introduce negative Gauss curvature. Following the original work of Caspar and Klug, we first construct models capable of reproducing the shape observed in Electron Microscopy images of archaeal viruses. Next, using the technique of Kirigami, we present a systematic way to formulate archaeal virus templates from regular hexagonal lattices. Finally, we utilize the presented techniques to build finite element models of archaeal virus geometries and investigate their shapes as a function of material properties. In particular, using thin-shell elasticity theory, we describe a buckling transition as a function of a modified Föppl von Kármán number $\gamma^\star$ and we show how changes in $\gamma^\star$ may initiate the tail formation in the *Acidianus* two-tailed archaeal virus.

I.   INTRODUCTION.

In 1962, Caspar and Klug (CK) [1] proposed a classification method for *viral capsids*, the protein shells that surround the genomes of viruses. Capsids have typical sizes in the range of 10-100 nm and are composed of hundreds of proteins, known either as capsid proteins or subunits. In the simplest case, the subunits are all identical. The CK construction is shown in Fig. 1. It consists of the cutting and pasting together of a template, which transforms a hexagonal sheet into a closed icosahedral shell. The reason that the construction has to start from a hexagonal lattice is that capsid proteins tend to crystallize into hexagonal sheets when they self-assemble on a flat surface.

The CK template is composed of twenty adjacent equilateral triangles of a hexagonal sheet (Fig 1). The base of each triangle is a lattice vector $\mathbf{A}(h, k) = h\mathbf{a_1} + k\mathbf{a_2}$ of the hexagonal lattice, with $\{h, k\}$ a pair of positive integers and $\{\mathbf{a_1}, \mathbf{a_2}\}$ a pair of basis vectors of the hexagonal lattice. The icosahedron is obtained by past-

[*] luigiemp@ucla.edu

[†] kszhang7@ucla.edu

[‡] Currently in the Department of Mechanical Engineering, Stanford University, Stanford, CA 94305, USA

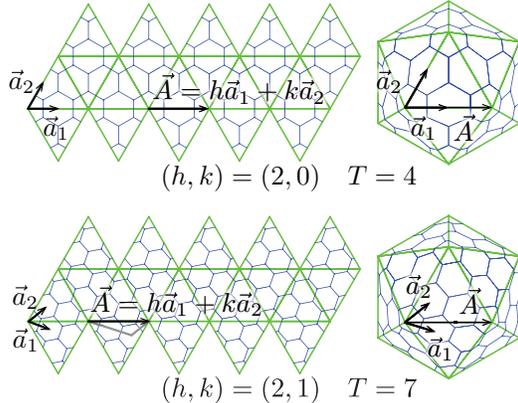[§] jarudnick@physics.ucla.edu

[¶] bruinsma@physics.ucla.edu

FIG. 1. (Color online) Caspar-Klug construction of icosahedral viruses. The basis vectors $\mathbf{a}_1$ and $\mathbf{a}_2$ of a two-dimensional hexagonal lattice are used to construct a template made of twenty equilateral triangles. Icosahedral shells can be constructed by folding the templates along the edges of the equilateral triangles and gluing them together. Depending on the steps h and k in the $\mathbf{a}_1$ and $\mathbf{a}_2$ directions, achiral (e.g., $T = 4$ with $h = 2$, $k = 0$ — top) or chiral (e.g., $T = 7$ with $h = 2$, $k = 1$ — bottom) shells can be formed. Figure reprinted from [2] (copyright 2015) with permission from Elsevier and composed using figures obtained from VIPERdb (http://viperdb.scripps.edu) [3]

ing together adjacent exposed edges of the template and hexamers at the border of a triangle neatly match with the hexamers of the triangle to which they will be attached. Examination of the shells of Fig. 1 shows that there are twelve pentamers at the vertices of the icosahedron. The construction can be repeated for every pair of integers h and k. Fig. 1 shows the construction of an achiral shell ($T = 4$ with $\{h, k\} = \{2, 0\}$) and of a chiral shell ($T = 7$, with $\{h, k\} = \{2, 1\}$). The size of an icosahedron is determined by the length of the base vector $\mathbf{A}(h, k)$. It follows from simple geometry that $|\vec{A}(h, k)|^2$ equals $T(h, k) = h^2 + k^2 + hk$, where T represents the capsid T number and characterizes the Caspar-Klug icosahedron.

By varying the size and shape of the template, the CK construction has been generalized to spherocylindrical and conical capsid shapes [4], encountered with retroviruses. However, there are viruses whose capsids appear to be beyond the reach of the CK construction. For example, the tiling of polyoma virus [5], simian virus 40 [6], and L-A virus [7] capsids require a different tiling approach as presented by Twarock [8, 9]. A different family of examples belong to the *Archaeal viruses*, a group of viruses that prey on the *Archaea* [10], prokaryotes that resemble more familiar bacteria in size and shape. However, their metabolism resembles that of plant and animal cells. Other properties, such as the structure of their membranes, appear to be unique to the *Archaea*. Archaeal viruses are an equally unusual family of double (ds) or single-stranded (ss) DNA viruses that infect the *Archaea*. We will focus here on a group of Archaeal viruses that are typified by the *Acidianus* two-tailed virus (ATV), a spindle-shaped archaeal virus (Fig. 2) that functions in acidic and hot environments [11, 12]. The reason that ATVs have morphologies that cannot be classified according to the standard CK method is that, exceptionally, their capsids have regions of *negative Gauss curvature*.

When the ATV virus assembles — under *in-vitro* conditions — at lower temperatures the tails are absent. The tails grow spontaneously if the temperature is increased above $75°C$ (Fig. 2) [11]. These extensions, or tails, are believed to play a role in establishing contact with potential host cells and it appears that tails are covered by the same layer of capsid proteins that constitutes the main body of the capsid.

The fundamental new feature of the ATV capsid in terms of crystallography is the presence of the sections of negative Gauss curvature where the two tails are connected to the main body of the virus. Shells constructed by the CK method have strictly positive Gauss curvature. For the CK method to apply to ATV and other archaeal viruses, it has to be generalized. Developing such a generalization is the first aim of this paper. A second aim is to examine whether tail assembly can be understood within the CK approach. To that purpose, we will build finite-element models of ar-
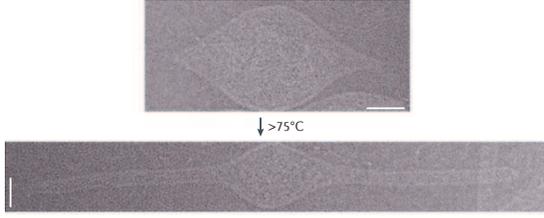
FIG. 2. ATV conformational change: from the tail-less lemon-shaped virion (top) to the tailed particle (bottom). Scale bars are 50 nm long. Adapted by permission from Springer Nature [13], copyright (2006). Originally adapted from [11].

chaeal viruses to study their *buckling instabilities*.

II. LATTICE KIRIGAMI FOR CLOSED SHELLS

Our approach is motivated by the three-dimensional structures that can be generated by cutting templates from two-dimensional lattices, an art form known as *Lattice Kirigami*[14]. Structures with negative Gauss curvature can indeed be generated by Lattice Kirigami but not within the confines of the CK rules. We specialize our form of Lattice Kirigami to hexagonal lattices. The basic construction units are then hexamers, pentamers, and heptamers (Fig. 3a). Starting from the hexamer units with zero Gauss curvature, the removal or addition of one triangular subunit produces units with positive (pentamers) and negative (heptamers) Gauss curvature, respectively.

Hexamers and pentamers are the standard units of the CK construction. Inclusion of the saddle-shaped heptamers allows the construction of shells with negative Gauss curvature. Figure 3b show a paper model example of a $T = 4$ CK capsid with a tail starting from a five-fold symmetry site where a pentamer was originally located. Heptamers link the tail to the body of the shell while pentamers close the end of the tail. In its most simple form (see
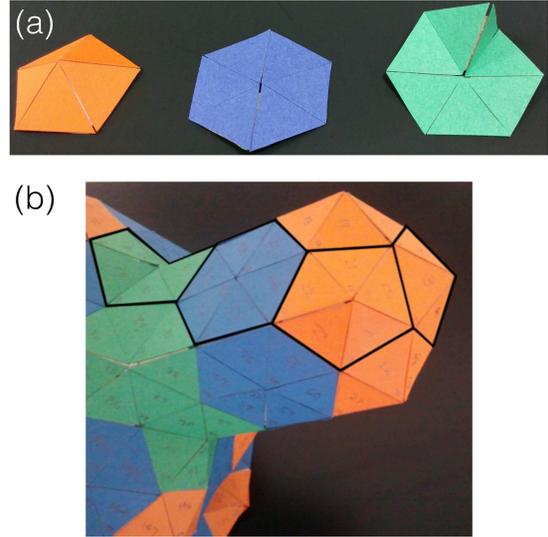

FIG. 3. (Color online) Paper models. a) Basic units: pentamers (orange), hexamers (blue), heptamers (green). b) Tail attached to a partial $T = 4$ CK capsid by a ring of heptamers. Several other paper model examples are included as supplemental material [15].

Fig. 4), one removes a pentamer plus a ring of five attached hexamers from the icosahedral shell. Then insert a ring of five heptamers to replace the hexamers and form the neck region. Subsequently, several five-fold symmetric rings of hexamers can be attached to the heptamers' ring to elongate the tail. Finally, a cap of *six* pentamers is used to close the end of the tail. Adopting the convention of assigning a +1 topological charge to pentamers and a −1 charge to heptamers, the net charge of the tail is +1, which is the same as that of the original pentamer. More generally, application of Euler's formula to a closed surface of pentamers, hexamers, and heptamers leads to the result that the net topological charge of the surface must equal 12. It follows that every additional heptamer must be balanced by adding an extra pentamer. In the simple case illustrated in Fig. 4 and discussed above, the five heptamers introduced in the neck regions are balanced by five additional pentamers added to the tail cap.
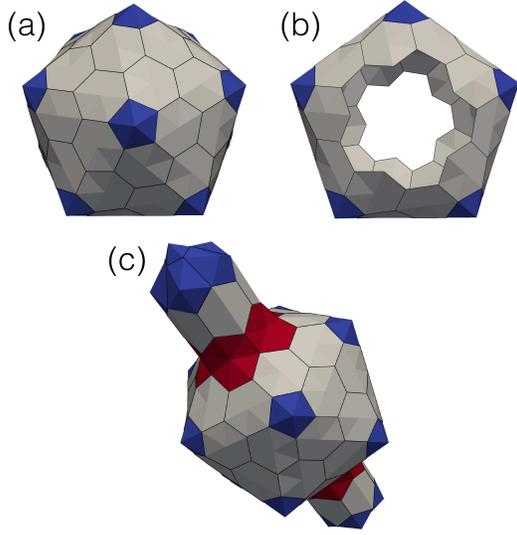
FIG. 4. (Color online) Construction of an ATV-like geometry starting from a CK icosahedral shell. In this example we use a $T = 7$ central body (a), remove a pentamer and its nearest ring of hexamers (b), and replace them with a five fold symmetric tail (c). Five heptamers are inserted at the base of the tail to introduce the negative Gauss curvature in the transition region from the central icosahedral body.

This construction can be repeated for any T number of the central body (e.g., see Fig. 5).

We can extend the same construction principle to non-icosahedral bodies (e.g., Fig. 6). For example, starting from an icosahedral shell, we can rotate one half of the capsid with respect to an axis passing through a three-fold symmetry site (i.e., the center of one face of the icosahedron) and introduce a mirror symmetry plane disrupting the icosahedral symmetry of the central body (Fig. 6a). Further variations containing two-fold symmetric tails are possible (e.g., Fig. 6b-c). In the latter examples, four heptamers are necessary in each neck region and six pentamers are present in the tails' caps. Although differently distributed in the capsid central body and tails, the total topological charge is still equal to $+12$ as expected by Euler's formula.
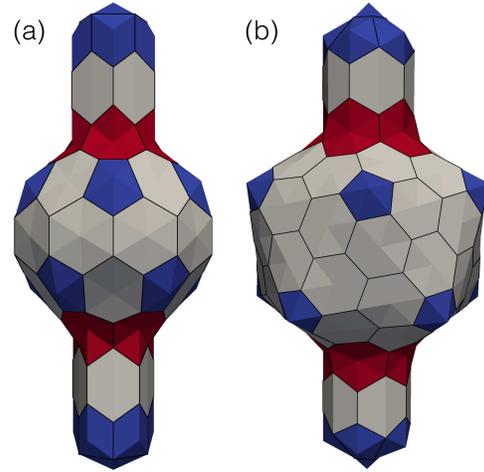

FIG. 5. (Color online) ATV-like geometries with $T = 4$ (a) and $T = 7$ (b) central icosahedral bodies. Several additional five-fold hexamer rings can be added to elongate the tethers' central sections.
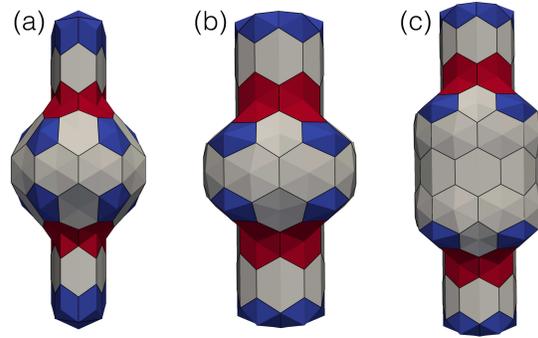

FIG. 6. (Color online) ATV-like geometries with non-icosahedral bodies. (a) Mirror symmetric capsid with five fold symmetric tail. (b-c) Two fold symmetric tethers connected with a single (b) and multiple (c) rings of hexamers in the central bodies.

Can one reproduce the shape of the ATV shell by this method? Increasing the T-number of the central body in Fig. 5 without modifying the tails results in a sharper transition between the central body and the tails, which does not reproduce the ATV capsid (e.g., see Fig. 2). Instead additional pentamer-heptamer pairs need to be introduced stepwise in order to gradu-

ally decrease the radius of the tails (Fig. 7). As more pairs are introduced, they begin to connect and develop into pentamer-heptamer "scars" along the capsid. We observed similar pentamer-heptamer scar-like structures on the surface of an unduloid representing the ATV capsid [16]. By using five pentamer-heptamer pairs for each step in the radius change, it is possible for each section to preserves five-fold symmetry. This leads to a key observation: the capsid can be approximated by stacking *locally* icosahedral sections separated by additional tail material. In the construction shown in Fig. (7, a), the capsid progresses from a $T = 9$ body to a $T = 4$ intermediate section and finally to a $T = 1$ cap.

It is important to notice that the long pentamer-heptamer scars in Fig. 7 are a result of how close the T-numbers of different sections are. As the size of the capsid grows, larger T numbers are recruited. In these larger T numbers, the five-fold sites are separated by a greater distance. As a result, the inserted pentamer-heptamer pairs are no longer adjacent to form a continuous "scar" and additional material is expected to appear in between each pentamer-heptamer pair.

III.   EXTENSION OF THE CASPAR-KLUG CONSTRUCTION TO ARCHAEAL VIRUSES

Using several examples, in Section II we have illustrated how ATV-like shapes can be constructed using pentamers, hexamers, and heptamers. In the following we want to formally extend the CK construction to form ATV-like shapes with icosahedral bodies from a planar hexagonal lattice. We begin by considering a single connection from the central icosahedral body to a tail of a certain size (e.g., Fig. 5). Subsequently we consider tails of varying radius such as the one presented previously in Fig. 7a.

We construct the partial icosahedral central body using the classic CK construction briefly reviewed in Section I and illustrated in Fig. 1. Accordingly, pentamers are placed at the ver-
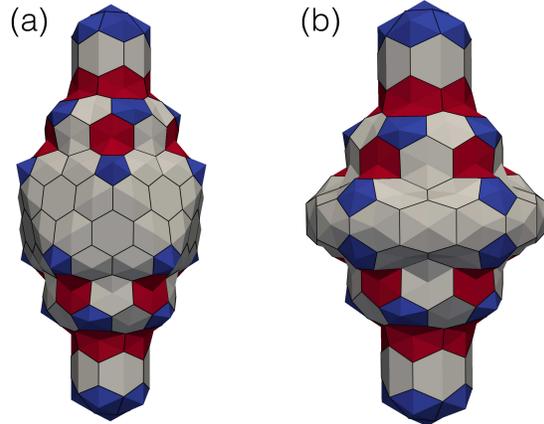

FIG. 7. (Color online) Gradually changing tail radius with icosahedral (a) or non-icosahedral (b) central bodies. By using heptamer/pentamer pairs we can gradually change the radius of the constructed ATV-like shells. As a result of the change in radius, pentamer/heptamer scars may develop in the tethers.

tices of the icosahedron identified by the (h, k) pair on the hexagonal lattice. In order to include the necessary negative Gauss curvature in the connection region between the tails and the central icosahedral body, we introduce heptamer units. Since the capsid is a closed surface, per each heptamer introduced in the connection region, there is a corresponding additional pentamer so that the net topological charge is preserved and equal to $+12$ as prescribed by Euler formula (See also [14] for general kirigami rules on a honeycomb lattice.)

In order to codify our construction and the location of the heptamer units, we start from the work presented in [4] for spherocylindrical viruses and define the following vectors (see Figs. 8, 9, and 10):

$$\mathbf{A} = m\mathbf{a}_1 + n\mathbf{a}_2 ; \tag{1a}$$

$$\mathbf{b}_1 = -\mathbf{a}_1 + 2\mathbf{a}_2 ; \tag{1b}$$

$$\mathbf{b}_2 = -2\mathbf{a}_1 + \mathbf{a}_2 ; \tag{1c}$$

$$\mathbf{B} = p\left(m\mathbf{b}_1 + n\mathbf{b}_2\right) . \tag{1d}$$

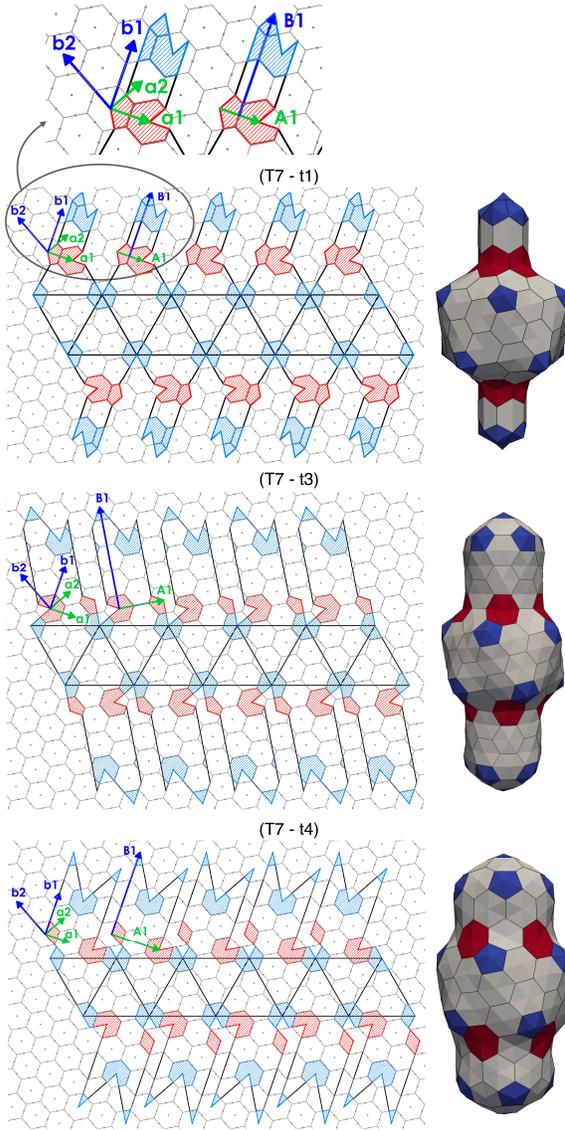The integers m and n represent the steps on the hexagonal lattice in the neck region between

FIG. 8. (Color online) Templates to construct ATV-like geometries with $T = 7$ icosahedral body and $t = 1$, $p = 1.5$ (top), $t = 3$, $p = \frac{4}{3}$ (center), and $t = 4$, $p = 1$ (bottom) tails. The 3D capsid corresponding to each template is shown on the right. We report the lattice vectors $\mathbf{a}_1$ and $\mathbf{a}_2$ together with the vectors $\mathbf{b}_1$, $\mathbf{b}_2$, $\mathbf{A}$, and $\mathbf{B}$ used to determine the tail t number and length.
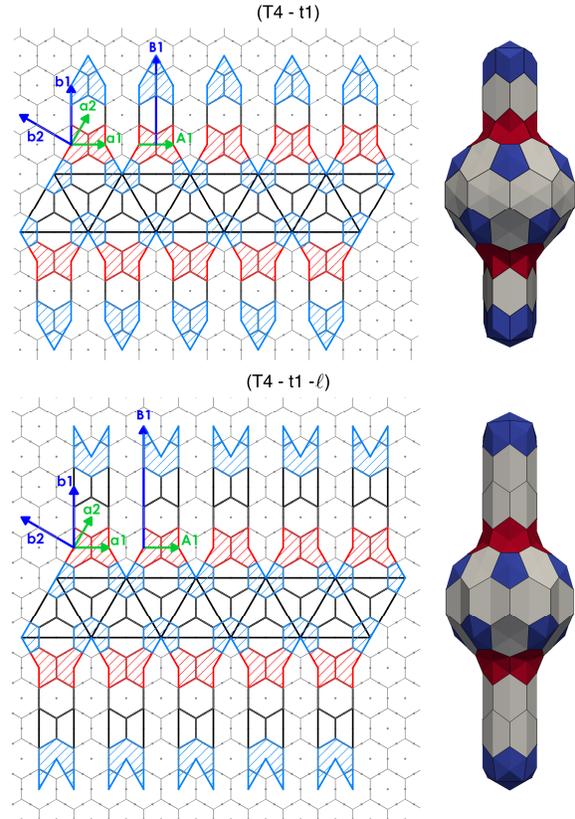

FIG. 9. (Color online) Templates to construct ATV-like geometries with $T = 4$ icosahedral bodies and $t = 1$ tails. The two templates correspond to different tail lengths and possible orientations of the tails' cap with respect to the icosahedral body ($p = 1.5$ top, $p = 2$ bottom). The lattice vectors $\mathbf{a}_1$ and $\mathbf{a}_2$ are shown together with the vectors $\mathbf{b}_1$, $\mathbf{b}_2$, $\mathbf{A}$, and $\mathbf{B}$ used to determine the tail t number and length.

two close heptamers. Accordingly the vector $\mathbf{A}$ connects two heptamers. As before (see Section I and Fig. 1) $\mathbf{a}_1$ and $\mathbf{a}_2$ are the basis vectors of the hexagonal lattice. The tail grows in the direction identified by the vector $\mathbf{B}$ to a length depending on p, with $p > 0$ (the tail cannot have zero length). Accordingly the vector $\mathbf{B}$ connects a heptamer in the transition region to the terminal pentamer at the center of the cap. The vector $\mathbf{B}$ is defined based on $\mathbf{b}_1$ and $\mathbf{b}_2$, which are orthogonal to $\mathbf{a}_1$ and $\mathbf{a}_2$, respectively.
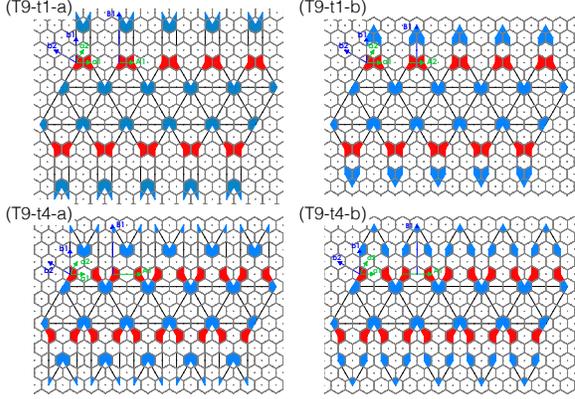
FIG. 10. (Color online) Templates to construct ATV-like geometries with $T = 9$ icosahedral body and $t = 1$ (top) and $t = 4$ (bottom) tails. For both t-number tails, we show the template corresponding to two possible orientations of the cap with respect to the icosahedral body: (T9-t1-a) $p = 2$, (T9-t1-b) $p = 1.5$, (T9-t4-a) $p = 1$, and (T9-t4-b) $p = 1$. Notice that both capsids (T9-t4-a) and (T9-t4-b) correspond to the same p number and have the same number of capsomers, although the cap orientation with respect to the central icosahedral body is different.

Based on the definition of vectors $\mathbf{A}$ and $\mathbf{B}$, we list a few principles governing our extension of the CK construction to archaeal viruses:

1. Each tail is five fold symmetric and can be classified by: 1) an additional T-number t determined by the steps m and n necessary to join the seven-fold sites at its base; and 2) a number p determining the length of the tail.

2. Given an icosahedral body characterized by h and k lattice constants, we can build tails with t-numbers $t = m^2 + mn + n^2$ for any combination $m \leq h$ and $n \leq k$, with at least either m or n strictly less than their respective h or k.

3. Chiral and achiral tails can be generated from either chiral or achiral bodies. Chiral central bodies lead to a more complex planar templates, e.g., compare Figs. 8 (chiral) and, 9 or 10 (achiral).

In the classic CK construction, a shell is composed of $10(T-1)+12$ capsomers. According to our construction the total number of capsomers composing the ATV-like shell with tail of *fixed radius* is:

$$N_{\mathrm{cpas}} = 10(T - 1) + 12 + 2(10p - 5)t . \quad (2)$$

Therefore the number of pentamers, hexamers, and heptamers is:

$$N_{\mathrm{pent}} = 22 ; \quad (3a)$$
$$N_{\mathrm{hex}} = 10(T - 3) + 2(10p - 5)t ; \quad (3b)$$
$$N_{\mathrm{hept}} = 10 . \quad (3c)$$

Our construction can be seamlessly extended to tails of varying radius. Each section i of fixed radius will be described by a set of constants (m_i, n_i, p_i): (m_i, n_i) will join adjacent heptamers at the base of the section i and p_i will describe the length of the tail section, from the heptamers at the base of the section to the position of the terminal pentamer if the tail would terminate with the current section (See Fig. 11).

If we allow for tails of varying radius, eqn. (2) can be generalized to:

$$N_{\mathrm{cpas}} = 10(T-1) + 12 + 2\sum_{i=1}^{N_t}(10p_i - 5)t_i , \quad (4)$$

where N_t is the number of tail segments with different radius, each with T number t_i and length determined by the vector B_i.

In the current algorithm, we have considered shells with the same tail size and length, but our construction can be easily extended to shells with tails of different size and length or shells with one tail only. These extensions can be achieved by introducing constants m, n, and p different for each tail and accordingly modifying eqns. (2), (3), and (4).

IV. ELASTICITY THEORY APPLIED TO ARCHAEAL VIRAL CAPSIDS

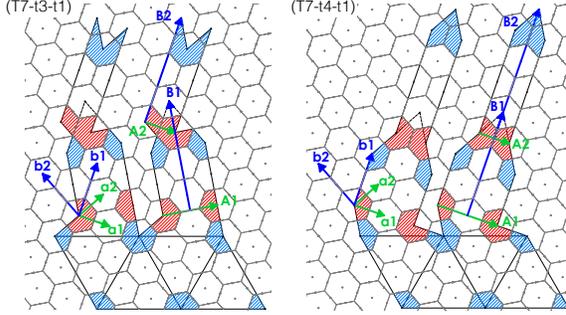We noted in the introduction that tailed archaea viral capsids can change their shape by

FIG. 11. (Color online) Templates to construct ATV-like geometries with tails of varying radius. Starting from a $T = 7$ icosahedral body, two tails of varying radius are shown: $(t_1 = 3, p_1 = \frac{7}{6})$ – $(t_2 = 1, p_2 = 2)$ tail (left) and $(t_1 = 4, p_1 = 1)$ – $(t_2 = 1, p_2 = 2.5)$ tail (right). The vectors $\mathbf{A}_1$ and $\mathbf{A}_2$ determine the subsequent tail t numbers while the vectors $\mathbf{B}_1$ and $\mathbf{B}_2$ characterize the tails length.

extending one or two tail groups (see Fig.2). The extension appears to be driven by the growth of a central fiber. Can such an extension be understood within the generalized CK construction? Shape changes of elastic shells are possible. A spherical shell can transform into a polyhedral shell under a change of the ratio of two-dimensional Young's Modulus Y and the bending modulus κ_c, which is known as the buckling transition as described by Lidmar et al. [17] for spherical capsids. Could a buckling-type transition be responsible for the tail growth? In order to answer this question, we applied thin shell elasticity theory to the models built according to the construction of Section III.

Following the work of Lidmar et al. [17] and our previous work [2], we divide the shell elastic energy Π into bending Π_b and in-plane Π_s energies:

$$\Pi = \Pi_b + \Pi_s ; \tag{5a}$$

$$\Pi_b = \int_\Omega \frac{\kappa_c}{2}(2H)^2 + \kappa_G K \, d\omega ; \tag{5b}$$

$$\Pi_s = \int_\Omega \frac{\kappa_s}{2}(J-1)^2 + \frac{\mu}{2}\left(\frac{\mathrm{tr}(C)}{J} - 2\right) d\Omega , \tag{5c}$$

where Ω is the shell surface, κ_c and κ_G are the bending and Gauss curvature moduli, H and K are the mean and Gauss curvatures, κ_s and μ are the 2D in plane stretching and shear moduli, J is the ratio between deformed and reference area, and C is the right Cauchy-Green deformation tensor. The split in area-stretching and shearing deformation in Π_s was proposed by [18].

The reference configuration for our calculations is the flat hexagonal lattice and therefore we do not introduce any intrinsic curvature in the expression of the bending energy. According to the Gauss-Bonnet theorem, the integral of the Gauss curvature over a closed surface is constant. Therefore, in our simulations the term $\int_\Omega k_G K \, d\omega$ in eq. (5b) integrates to a constant value equal to $4\pi\kappa_G$ and it does not affect the final shape attained by the capsid.

We model the capsid deformation according to Kirchhoff-Love thin shell theory. We minimize the shell energy Π by discretizing the capsid with non-local C^1 continuous Loop shell finite elements [19, 20] to minimize the bending energy Π_b, and with linear triangular elements to minimize the in plane energy Π_s.

We initialize our simulations by: 1) projecting radially all the vertices of the shell triangular mesh onto a unit sphere; 2) computing the average edge length $\bar{\ell}$ of the mesh projected on the unit sphere; and 3) setting the triangular elements *reference* edge length equal to $\bar{\ell}$. This initialization enforces that all triangular elements forming the elastic shell have the same flat equilateral triangle as reference configuration from which the in plane energy Π_s is computed.

The energy of the finite element model is minimized using the LBFGS solver [21]. A detailed description of the finite elasticity model and numerical methods used herein can be found in [2].

We analyze the shell shape as a function of a modified Föppl von Kármán (FvK) number and shell asphericity. The FvK number characterizes the ratio between shell stretching and bending stiffness. The shell asphericity instead characterizes the shell shape with respect to a perfect sphere. For spherical – or almost spher-

ical – shells the Föppl von Kármán (FvK) number γ is defined as YR^2/κ_c, where R is the average shell radius and $Y = 2\kappa_s(1 - \nu)$ is the 2D Young modulus, with ν being the Poisson ratio. In our calculation we set $\nu = 0.3$. For non spherical shells for which R is not well defined, we extend the definition of the FvK number to $\gamma^\star = YA/\kappa_c$, where A is the shell current area $(A = \int_\Omega d\omega)$. Analogously, the definition of asphericity where R is well defined is $\frac{\langle \Delta R^2 \rangle}{\langle R \rangle^2}$ [17], where $\Delta R = R - \langle R \rangle$ and $\langle \cdot \rangle$ denotes the average over the shell surface. In our case, we adopt two alternative definitions of asphericity based on the mean H and Gauss K curvatures as $\frac{\int_\Omega (H - \langle H \rangle)^2 d\omega}{A}$ and $\frac{\int_\Omega (K - \langle K \rangle)^2 d\omega}{A}$.

Starting from the spherical reference configuration, in all simulations presented here we increase Y from 0.5 to 300 in 300 logarithmic increments while κ_c was held constant and equal to 1. Changes in Y corresponded to changes in $\gamma^\star$ from ≈ 4 to ≈ 3930. We emphasize that the capsid shape changes presented in the following are only due to changes in $\gamma^\star$ and no other parameters were modified in computing subsequent equilibrium configurations.

We simulated six representative shells that differ in T number of the central icosahedral body, t number of the tails, and tails' length. In Figures 12-17 we denotes with the following abbreviations the analyzed shells: $T9 - t4 - t1$ has an icosahedral $T = 9$ central body and gradually varying tail with t number 4 and 1 (Fig. 7, a); $T7 - t4$, $T7 - t3$, $T7 - t1$ are built with an icosahedral $T = 7$ central body and constant radius tails with t numbers 4, 3, and 1, respectively (Fig. 8); $T4 - t1$ and $T4 - t1\ell$ have an icosahedral $T = 4$ central body and constant radius $t = 1$ tails with different lengths — $p = 1.5$ in $T4 - t1$ and $p = 2$ in $T4 - t1\ell$ (Fig. 9).

Shortly after $\gamma^\star$ begins to increase from the initial configuration, the shells asphericity undergoes a sharp transition (Figures 12, 13). This sharp increase in both Gauss and mean curvature based asphericities correspond to the tail growth from the central body (Figures 14, 15, and 16). As $\gamma^\star$ increases, the tails continue to extend and the shell shape encoded in the

flat regular hexagonal templates are expressed. These findings are consistent in all the simulations carried out with the representative shells listed above. Figure 17 shows the shell transformation along the tail axis. At low $\gamma^\star$ (top row), it is apparent the template pattern from which the shells are built and that encodes the shells final shapes. As $\gamma^\star$ increases, the Gauss curvature becomes negative in the neck regions and increases at the tail ends. See supplemental material [15] for videos of tails' growth as a function of increase in FvK number $\gamma^\star$ for the cases presented in Figs. 14 to 17.
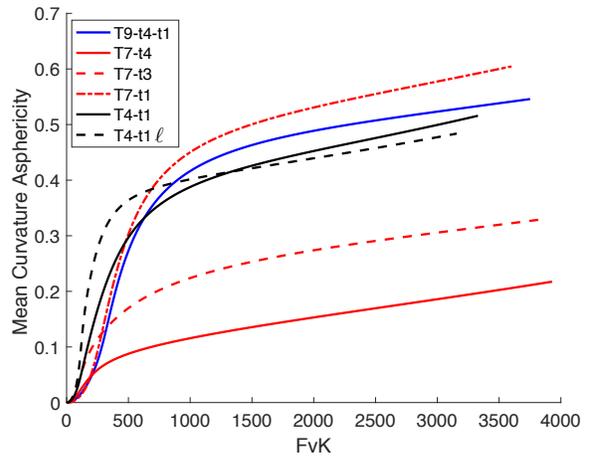

FIG. 12. (Color online) Mean curvature asphericity $\left(\frac{\int_\Omega (H - \langle H \rangle)^2 d\omega}{A} \right)$ as a function of FvK number $\gamma^\star$ (YA/κ_C) for ATV-like capsids built using $T = 4$, $T = 7$, and $T = 9$ central bodies.

We notice that the results presented here have been obtained without enforcing a constant area constraint. However, the same calculations carried out imposing an area constraint lead to similar results.

V. CONCLUSION

In this work we have proposed an algorithm to construct closed shells with positive and negative Gauss curvature as the ATV capsid. Our construction algorithm is an extension of the
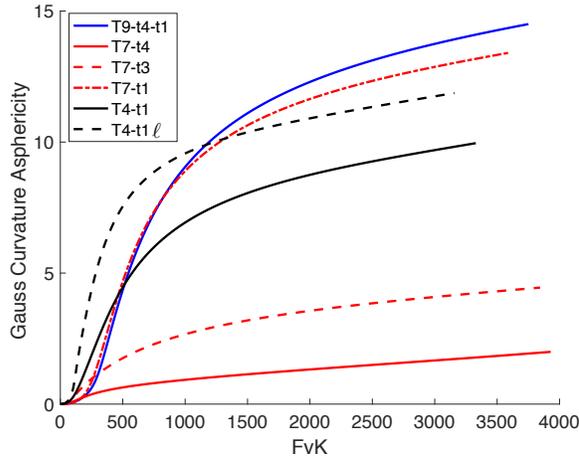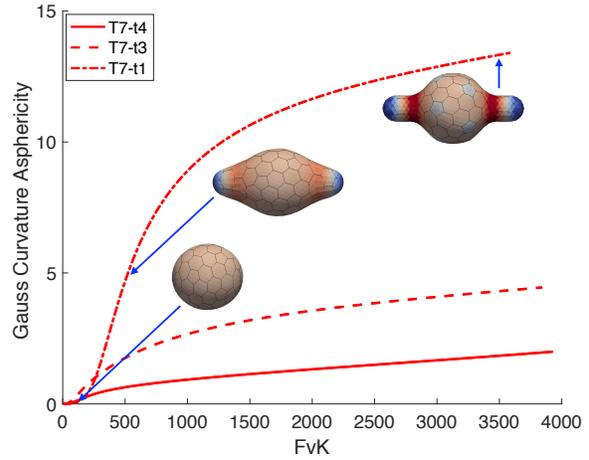
FIG. 13. (Color online) Gauss curvature asphericity $\left(\frac{\int_\Omega (K - \langle K \rangle)^2 d\omega}{A}\right)$ as a function of FvK number $\gamma^\star$ (YA/κ_C) for ATV-like capsids built using $T = 4$, $T = 7$, and $T = 9$ central bodies.

FIG. 15. (Color online) Gauss curvature asphericity $\left(\frac{\int_\Omega (K - \langle K \rangle)^2 d\omega}{A}\right)$ as a function of FvK number $\gamma^\star$ (YA/κ_C) for ATV-like capsids built using $T = 7$ central body. Insets illustrate capsid configuration at representative FvK numbers equal to ≈ 50, ≈ 500, and ≈ 3500.
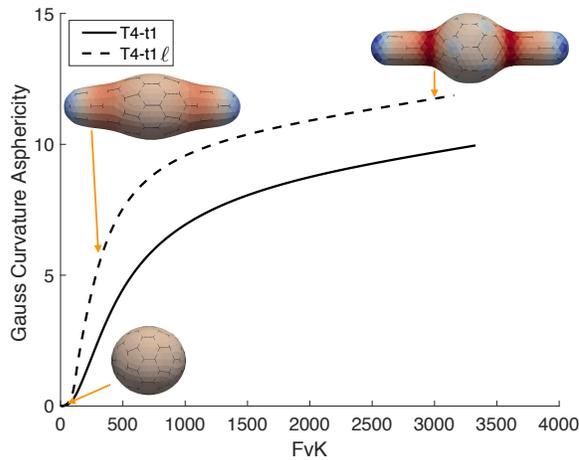

FIG. 14. (Color online) Gauss curvature asphericity $\left(\frac{\int_\Omega (K - \langle K \rangle)^2 d\omega}{A}\right)$ as a function of FvK number $\gamma^\star$ (YA/κ_C) for ATV-like capsids built using $T = 4$ central body. Insets illustrate capsid configurations at representative FvK numbers equal to ≈ 30, ≈ 300, and ≈ 3000.
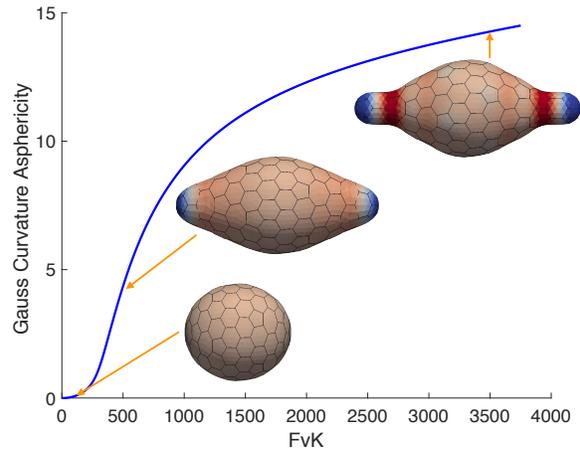

FIG. 16. (Color online) Gauss curvature asphericity $\left(\frac{\int_\Omega (K - \langle K \rangle)^2 d\omega}{A}\right)$ as a function of FvK number $\gamma^\star$ (YA/κ_C) for ATV-like capsids built using $T = 9$ central body. Insets illustrate capsid configuration at representative FvK numbers equal to ≈ 50, ≈ 500, and ≈ 3500.

classic Caspar-Klug construction and is based only on three basic units: pentamers, hexamers — as in the Caspar-Klug construction with only positive Gauss curvature — and heptamers
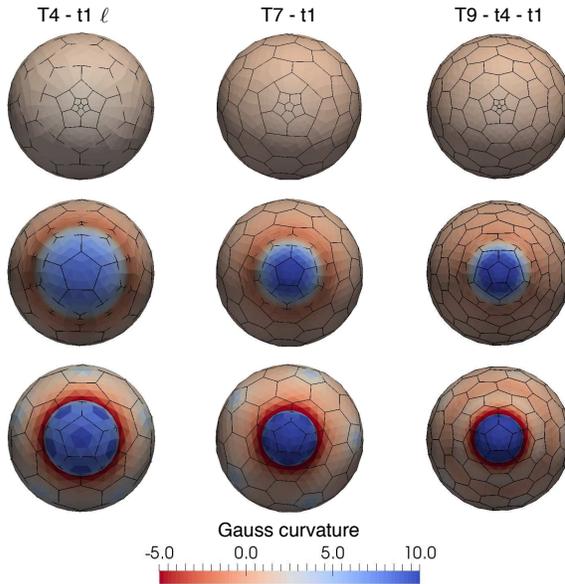
FIG. 17. (Color online) Shape evolution of ATV-like capsids built with $T = 4$ (left), $T = 7$ (center), and $T = 9$ (right) central bodies. These front views correspond to the lateral views reported in the insets of figures 14, 15, and 16, respectively, and illustrate the capsid configurations at representative FvK numbers equal to ≈ 50 (≈ 30 for $T4 - t1\,\ell$), ≈ 500 (≈ 300 for $T4 - t1\,\ell$), and ≈ 3500 (≈ 3000 for $T4 - t1\,\ell$). The shells are colored by Gauss curvature.

— necessary to introduce negative Gauss curvature. As in the Caspar-Klug construction, the topology of the ATV-like shell is completely defined by the number of steps along predefined directions over a regular hexagonal lattice that lead to the location of the five and seven fold type defects (e.g., see eq. (1)). Therefore the topology of the shell is easily codified by a list of steps and directions, and different prototypes can be easily classified and created.

Motivated by the buckling transition observed in spherical viruses, we explored whether such a transition existed for the ATV-like shells and whether it could explain tail formation. We showed that the buckling transition indeed can promote tail growth provided the negative Gauss curvature sections are "programmed in"

by a suitable distribution of heptamers (see Figures 14-16). The tail growth during the buckling transition is driven by a change in material properties, i.e., the modified Föppl von Kármán (FvK) number $\gamma^\star$. In other words, it requires that the virus regulates somehow the elastic moduli of the capsid. Is this possible? In fact, there are examples of viruses that modulate their own material properties leading to a buckling transition. A well known example is the HK97 virus [22] where a change in the bending modulus following a bond scission reaction produces buckling [23]. Whether this happens as well for ATV would have to be demonstrated. A separate way of testing the theory could be based on a micro-mechanical study that measured the resistance of the capsid against nano-indentation by an atomic-force microscope (AFM) [24], since the elastic response of a shell is quite different depending on whether the shell is in a liquid or a solid state. If tail growth is not due to a form of buckling, then the capsid would have to allow for a form of *flow* of capsid proteins during tail growth. This would require the capsid proteins to be in a fluid or smectic liquid-crystalline state [25] (one would need to understand how a fluid or liquid crystalline shell can withstand the large osmotic pressure that is known to be present inside ds DNA phage viruses in this explanation).

In summary, a shell with positive and negative Gauss curvature may be encoded in a regular hexagonal lattice by placing 5 and 7 types defects according to a precise construction. Subsequently, by increasing uniformly the ratio between in plane Young modulus and bending modulus, the shape initially encoded in the flat template can be expressed and, as part of the morphing process, tethers can extend from the central body.

tions in structural virology. His friendship and advices shaped our lives.

[1] D. Caspar and A. Klug, in *Cold Spring Harbor Symposia on Quantitative Biology*, Vol. 27 (1962) pp. 1–24.

[2] L. E. Perotti, A. Aggarwal, J. Rudnick, R. F. Bruinsma, and W. S. Klug, Journal of the Mechanics and Physics of Solids **77**, 86 (2015).

[3] M. Carrillo-Tripp, C. M. Shepherd, I. A. Borelli, S. Venkataraman, G. Lander, P. Natarajan, J. E. Johnson, C. L. Brooks III, and V. S. Reddy, Nucleic acids research **37**, D436 (2008).

[4] T.T. Nguyen, R. F. Bruinsma, and W. M. Gelbart, Physical Review E **72**, 051923 (2005).

[5] I. Rayment, T. Baker, D. Caspar, and W. Murakami, Nature **295**, 110 (1982).

[6] R. Liddington, Y. Yan, J. Moulai, R. Sahli, T. Benjamin, and S. Harrison, Nature **354**, 278 (1991).

[7] J. R. Castón, B. L. Trus, F. P. Booy, R. B. Wickner, J. S. Wall, and A. C. Steven, The Journal of cell biology **138**, 975 (1997).

[8] R. Twarock, Journal of Theoretical Biology **226**, 477 (2004).

[9] R. Twarock, Philosophical Transactions of the Royal Society of London A: Mathematical, Physical and Engineering Sciences **364**, 3357 (2006).

[10] C. R. Woese, O. Kandler, and M. L. Wheelis, Proceedings of the National Academy of Sciences **87**, 4576 (1990).

[11] D. Prangishvili, G. Vestergaard, M. Häring, R. Aramayo, T. Basta, R. Rachel, and R. Garrett, J. Mol. Biol. **359**, 1203 (2006).

[12] M. Häring, G. Vestergaard, R. Rachel, L. Chen, R. A. Garrett, and D. Prangishvili, Nature **436**, 1101 (2005).

[13] D. Prangishvili, P. Forterre, and R. Garrett, Nat. Rev. Microbiol. **4**, 837 (2006).

[14] T. Castle, Y. Cho, X. Gong, E. Jung, D. M. Sussman, S. Yang, and R. D. Kamien, Physical review letters **113**, 245502 (2014).

[15] "See Supplemental Material at [URL will be inserted by publisher] for 1) Additional examples of paper models to construct ATV-like shells; 2) Movies of tails' growth driven by an increase in FvK number.".

[16] L.E. Perotti, S. Dharmavaram, W.S. Klug, J. Marian, J. Rudnick, and R.F. Bruinsma, Physical Review E **94**, 012404 (2016).

[17] J. Lidmar, L. Mirny, and D. R. Nelson, Physical Review E **68**, 051910 (2003).

[18] E. Evans and R. Skalak, CRC critical reviews in bioengineering **3**, 181 (1979).

[19] F. Cirak, M. Ortiz, and P. Schroder, International Journal for Numerical Methods in Engineering **47**, 2039 (2000).

[20] F. Cirak and M. Ortiz, International Journal for Numerical Methods in Engineering **51**, 813 (2001).

[21] C. Zhu, R. H. Byrd, P. Lu, and J. Nocedal, ACM Transactions on Mathematical Software (TOMS) **23**, 550 (1997).

[22] J. Conway, W. Wikoff, N. Cheng, R. Duda, R. Hendrix, J. Johnson, and A. Steven, Science **292**, 744 (2001).

[23] A. Aggarwal, J. Rudnick, R.F. Bruinsma, and W.S. Klug, Physical review letters **109**, 148102 (2012).

[24] W. Roos, R. Bruinsma, and G. Wuite, Nat Phys **6**, 733 (2010).

[25] S. Dharmavaram, J. Rudnick, C. Lawrence, and R. Bruinsma, Journal of Physics: Condensed Matter **30**, 204004 (2018).